Absolute cross sections for near-threshold electron-impact excitation of Be-like C^{2+}, N^{3+}, and O^{4+} ions

M. E. Bannister

Physics Division, Oak Ridge National Laboratory, Oak Ridge, TN 37831-6372, USA

N. Djurić, O. Woitke, and G. H. Dunn

JILA, University of Colorado and NIST, Boulder, CO 80309, USA

Y.-S. Chung

Chungnam National University, 305-764 Daejon, South Korea

A.C.H. Smith

Department of Physics and Astronomy, University College London, London WC1E 6BT, UK

B. Wallbank

St. Francis Xavier University, Antigonish, Nova Scotia, Canada B2G 2W5

K. A. Berrington

School of Science and Mathematics, Sheffield Hallam University, Sheffield S1 1WB, UK

Abstract

Absolute total cross sections for electron-impact excitation of the Be-like C^{2+}, N^{3+} and O^{4+} ions have been measured near threshold using the merged electron-ion beams energy-loss (MEIBEL) technique and calculated using a close-coupling R-matrix (CCR) approach. The $2s^2\ {}^1S \rightarrow 2s2p\ {}^1P^o$ dipole-allowed transition from the ground state was investigated for all three ions and satisfactory agreement between experiment and theory is found. In addition, calculations and measurements for the $2s2p\ {}^3P^o \rightarrow 2p^2\ {}^3P$ allowed transition from the metastable level of C^{2+} are in excellent agreement. The sum of the cross sections for the $2s^2\ {}^1S \rightarrow 2s2p\ {}^3P^o$ and $2s2p\ {}^3P^o \rightarrow 2s2p\ {}^1P^o$ spin-forbidden transitions, not completely resolved by the MEIBEL technique, are measured for C^{2+} and O^{4+} and compared to CCR calculations scaled to account for the ground state and metastable fractions of the target ion beams. The results for these unresolved transitions are in reasonable agreement except for a resonance feature measured in the 2s2p $^3P^o \rightarrow$ 2s2p $^1P^o$ transition in C^{2+} that is not predicted by theory.

1 Introduction

In most plasma environments the properties are determined by the electrons and the ions, and the interactions between them. Inelastic electron-ion collisions play a major role in the energy balance of plasmas. For this reason, modelers and diagnosticians require absolute cross sections for these processes. Cross sections for electron-impact excitation of ions are needed to interpret spectroscopic measurements and for simulations of plasmas using collisional-radiative models.

Ions in the beryllium isoelectronic sequence are present in a range of laboratory and astrophysical plasmas including fusion devices [1], planetary nebulae [2,3], and active galactic nuclei [4,5]. Emissions from transitions among the $n = 1$ and $n = 2$ levels of various ions are the primary spectral lines observed in such plasmas. Accurate excitation cross sections for these transitions are required for proper interpretation of the observed spectra. A recent paper [6] reviews the current status of excitation data for C^{2+}, N^{3+}, O^{4+}, and other Be-like ions.

For dipole-allowed excitations, the primary contribution to the cross section is from direct excitation. For spin-forbidden transitions, however, the direct contribution may be relatively small so that the near-threshold excitation cross sections are commonly dominated by dielectronic resonances [7–11]. These resonances arise from resonant capture of incident electrons to doubly-excited levels of the next-lower charge state of the ion followed by autoionization to an excited level of the original charge state. Resonances seen in dielectronic recombination of ions follow this same mechanism except stabilization of the doubly-excited ion is accomplished through radiation instead of autoionization. Accurate *ab initio* calculations of the dielectronic resonance contributions to the excitation cross sections are difficult because theoretical approaches must attempt to describe the $(n + 1)-$electron system of the doubly-excited intermediary with $n-$electron wavefunctions of the target ion. Benchmark measurements of selected excitation systems and direct comparison with theory are crucial in the attempt to provide accurate data for modeling and diagnosing of plasmas.

In this paper, we present electron-impact excitation cross sections for Be-like C^{2+}, N^{3+}, and O^{4+} ions measured using the merged electron-ion beams

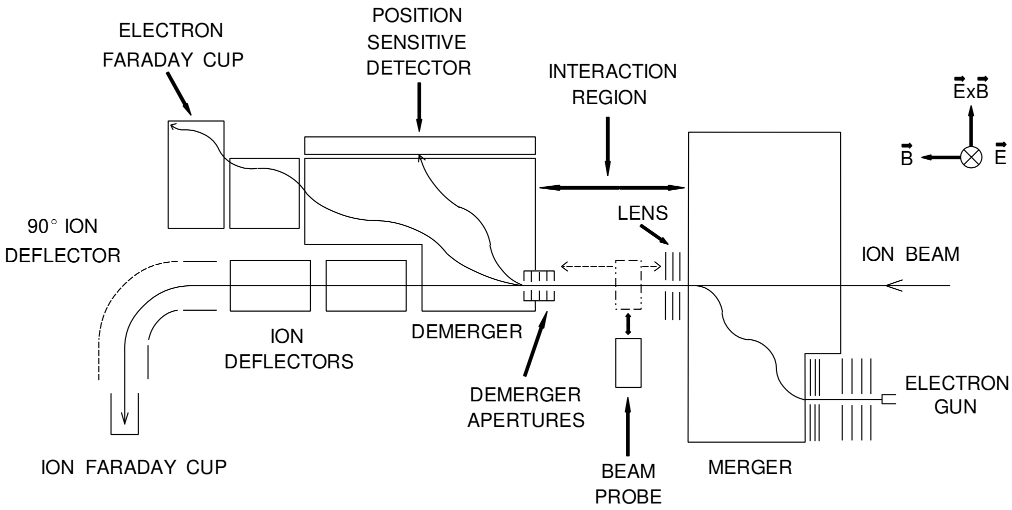

Fig. 1. Schematic diagram of the merged electron-ion beams energy loss apparatus (see text for description).

energy-loss (MEIBEL) technique [12,13] and calculated with a close-coupling R-matrix (CCR) approach [14]. Theory and experiment are compared for both dipole-allowed and spin-forbidden excitations from the $2s^2\ ^1S$ ground state as well as the 2s2p $^3P^o$ metastable level.

2 Experiment

The MEIBEL technique is based on the detection of low-energy electrons that have been inelastically scattered from target ions. Many of the experimental details have been reported previously [15], so only a brief description will be given in this paper. The MEIBEL apparatus used for the present investigation is shown schematically in Fig. 1 and is immersed in a uniform solenoidal magnetic field parallel to the ion beam and defining the z-direction. Electrons are extracted from a dispenser-type cathode and focused into a beam in the electron gun. A trochoidal energy analyzer known as the “merger” (with crossed electric and magnetic fields) is adjusted so that the electrons traverse the crossed-fields region in two gyrations, leaving the merger with the same velocity vector as they entered, but displaced perpendicular to the magnetic field. In this way, the electrons can be merged with ions extracted from the ORNL Caprice electron-cyclotron-resonance (ECR) ion source. Upon leaving the merger, the ions and electrons drift together through the electric-field-free interaction region (or “merge path,” 68.5 mm long) before being separated by a second trochoidal analyzer, the “demerger.” The demerger electric field is set to deflect electrons that have been inelastically scattered in the excitation process of interest onto a position sensitive detector (PSD). This PSD is composed of two microchannel plates in tandem backed by a resistive anode. Unscattered electrons are deflected relatively less by the demerger fields and are collected in a Faraday cup. A set of apertures at the entrance of the demerger blocks electrons elastically scattered through large angles that would otherwise reach the PSD. The ion trajectories are relatively unaffected by the demerger, passing through to be deflected and then collected in another Faraday cup.

In order to extract the excitation signal from the large backgrounds produced by the two charged particle beams passing through the apparatus, both beams are chopped in a four-way phased chopping scheme [15]. The counts from the position computer are directed into four histogramming memories corresponding to (1) both beams on, (2) electron beam on, (3) ion beam on, and (4) both beams off. The counts in the four memories are individually corrected for dead times of the PSD and signal processing electronics. By combining these corrected counts, the two-dimensional inelastic signal received by the PSD can be reconstructed.

The excitation cross section at an interaction energy in the center-of-mass system, E_{cm}, is determined from measured quantities by

$$\sigma(E_{cm}) = \frac{qe^2}{\varepsilon}\left|\frac{v_e v_i}{v_e - v_i}\right|\frac{R}{I_e I_i}F, \tag{1}$$

where ε is the PSD detection efficiency measured to be 0.445 ± 0.018, v_e, v_i, I_e and I_i are the laboratory velocities and currents of the electrons and ions of charge magnitudes e and qe, respectively, and R is the signal count rate from detection of the inelastically scattered electrons. The form factor, F, is given by

$$F = \frac{\int G(x,y,z)dxdy \int H(x,y,z)dxdy}{\int G(x,y,z)H(x,y,z)dxdydz}. \tag{2}$$

The densities of the two beams, $G(x,y,z)$ and $H(x,y,z)$, are measured with a movable video probe [16] at several positions along the interaction region. The probe consists of a microchannel plate backed by a phosphor-coated coherent fiber optic bundle to convert the incident particles into an optical signal that is then detected by a charge-injection device camera chip.

The data-taking protocol requires that the laboratory energy of the electrons be selected to give the desired center-of-mass energy for a given ion energy using

$$E_{cm} = \left[\sqrt{\left(1 + \frac{m_e}{m_i}\right) E_{lab}} \; - \; \sqrt{\frac{m_e}{m_i} E_i} \; \right]^2 \tag{3}$$

where E_{lab} and E_i are the laboratory energies of the electrons and ions of mass m_e and m_i, respectively. The beams are then tuned to minimize their individual backgrounds and optimize their overlap in the interaction region. The beams are arranged to prevent overlap within or beyond the demerger apertures since large-angle elastic scattering events in these regions could produce spurious signal on the detector. Once the form factor for a given beam arrangement has been measured with the beam probe, data taking begins at the first center-of-mass energy and continues until the required statistical accuracy is reached. Then E_{cm} is changed by scaling the voltages applied to the electrodes of the electron gun, merger, and demerger and the magnetic field for a new laboratory energy for the electrons. By scaling by only a few percent, the overlap of the two beams is reproduced at the new energy so that the previously measured form factor is still applicable. This process continues until the cross section has been measured over a certain range of E_{cm}. The beam overlaps are then remeasured to demonstrate that the form factor has remained constant within its experimental uncertainty for this set of data.

Despite the care taken to eliminate elastically scattered electrons from reaching the detector and to minimize the backgrounds associated with the two beams, a signal below the inelastic threshold is sometimes measured. This below threshold spurious signal is found to be independent of energy and is subtracted from data sets in which it is measured. For the dipole-allowed transitions, this correction is determined in the threshold fitting procedure described below. For the spin-forbidden transitions, the correction is determined from the variance-weighted mean of all measurements with energies more than 0.2 eV below the spectroscopic threshold.

The interaction energy scale is established with the dipole-allowed $2s^2\ ^1S \rightarrow 2s2p\ ^1P^o$ transition for each of the Be-like ions. The excitation cross sections measured for these transitions are fitted in the threshold region (defined as all energies up to 0.5 eV greater than the top of the excitation step) with the convolution of a step function and a Gaussian representing the experimental electron energy distribution. The least squares fit includes adjustable parameters for the step height, the full-width at half-maximum (FWHM) of the Gaussian, the energy shift from the spectroscopic value of the threshold, and the below-threshold spurious signal. This procedure therefore establishes the absolute energy scale of the experiment, shifts the measured threshold to the spectroscopic value, and accounts for the “contact potential” of the electron gun cathode. This is critical for comparison of resonance positions measured for spin-forbidden transitions with those predicted by theory. The determination of the FWHM of the electron energy distribution allows a more direct comparison of the measured cross sections with theoretical results.

Purity of the target ion beam is a particular concern in the present study. Isotopic ^{13}C and ^{18}O were used in the ECR ion source in order to reduce ion impurities with the same mass-to-charge ratios to less than 1% of the analyzed ion current. This same level of beam purity was achieved for N^{3+} using the naturally most abundant isotope, mass 14.

Metastable ions in the 2s2p $^3P^o$ state constitute a significant portion of Be-like ions extracted from ECR ion sources [17]. Lifetimes of these metastable ions [18,19] are much greater than the few microsecond flight time of ions from the source to the interaction region. Thus, one must account for the ground state and metastable fractions of the target ion beam in order to determine absolute cross sections for transitions from either of the states. Previous MEIBEL experiments involving metastables [10,11] in the incident ion beam relied on electron-impact ionization measurements [20] combined with theoretical predictions to determine the metastable fraction. The existing theoretical ionization cross sections [21] for the present Be-like ions, however, are not sufficiently accurate to reliably determine the metastable fraction by this method. Our crossed-beams electron-impact ionization measurements for C^{2+}, N^{3+}, and O^{4+} did indicate a significant fraction of ions in the metastable 2s2p $^3P^o$ state. In the absence of directly measured metastable fractions for the present ions, we have adopted the values measured by Brazuk *et al.* [17] for Be-like ions extracted from a similar ECR ion source. By measuring core-conserving electron capture from Li(2s), they determined metastable fractions of 0.56 ± 0.11, 0.52 ± 0.08, and 0.42 ± 0.06 for C^{2+}, N^{3+}, and O^{4+} ion beams, respectively. Our preliminary beam attenuation measurements for C^{2+} yielded a metastable fraction consistent with the value reported by Brazuk *et al.*

Just above threshold for a given transition, electrons scattered inelastically (hereafter referred to as "inelastic electrons") through 180 degrees in the CM frame are still traveling forward (+z direction) in the LAB frame with almost the center-of-mass velocity v_{cm}. At higher energies, however, inelastic electrons will travel backward in the LAB frame when their backward (-z direction) velocity component exceeds v_{cm}. Such electrons will not reach the detector, leading to loss of signal. There are additional signal losses possible as some electrons inelastically scattered forward in the LAB frame can miss the detector. Electrons with small forward velocities can be reflected by the electric field of the demerger during the downward portion of their trochoidal motion since below the ground plane of the demerger (typically about 0.5 mm below the geometric beam axis) electrons experience a retarding potential. Other inelastic electrons can be lost if their Larmor radii are large enough for their gyromotions to be intercepted by the demerger apertures. All of these

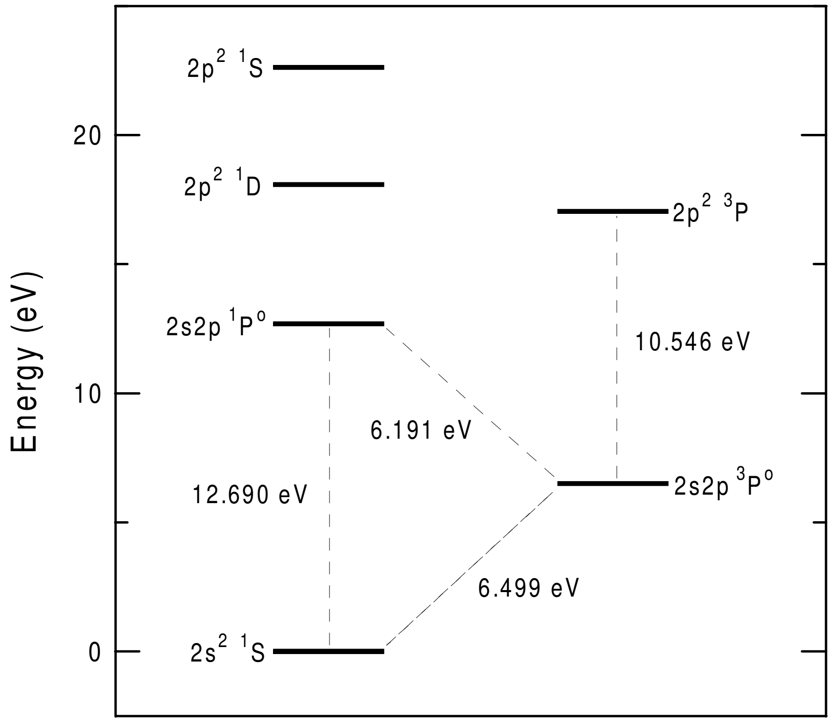

Fig. 2. Energy diagram for the $n = 2$ levels of C^{2+}. The energies are the statistically weighted multiplet averages of the values given in Ref. [23]. Transition energies are shown for the excitations of the present study.

losses can be estimated using a three-dimensional trajectory modeling program [22] taking into account the fields of the demerger and the position of the scattering events as determined by the measured beam overlaps. Weighting the trajectories that miss the detector according to scattering angle by using the appropriate differential scattering cross section (calculated with the CCR approach at a single energy about 1 eV above threshold), one can correct the measured signal for such losses. For the $2s^2\ ^1S \rightarrow 2s2p\ ^1P^o$ transitions, corrections to the measured cross sections start approximately 0.65 eV above threshold and are less than 5% except for the few highest energies measured. Similar corrections for backscattering and other losses were made for the other transitions measured.

Since the MEIBEL technique relies on detecting inelastically scattered electrons with an energy loss method, it cannot differentiate signal electrons arising from different excitations with nearly equal threshold energies. For the Be-like C^{2+}, N^{3+}, and O^{4+} ions, the 2s2p $^3P^o$ level lies just over half way between the $2s^2\ ^1S$ ground level and the 2s2p $^1P^o$ level. This is illustrated in Fig. 2, an energy diagram for the $n = 2$ levels [23] in C^{2+} showing the transitions of interest in the present study. At center-of-mass energies above the threshold for the excitation of the $^3P^o \rightarrow {}^1P^o$ transition (6.191 eV) and below that for the $^1S \rightarrow {}^3P^o$ transition (6.499 eV), all inelastic electrons reaching the detector must be the result of the $^3\mathrm{P}^o \rightarrow {}^1\mathrm{P}^o$ transition. But just above the $^1\mathrm{S} \rightarrow {}^3\mathrm{P}^o$ threshold, inelastic electrons from the $^3\mathrm{P}^o \rightarrow {}^1\mathrm{P}^o$ transition are also striking the detector so that the measured signal is the sum of signals from the two excitations.

The relative uncertainties of the measurements at the 90% confidence level are the quadrature sum of the statistical uncertainty with a coverage factor of $k = 1.7$, uncertainty arising from incomplete collection of the signal due to backscattering and demerger losses (20% of the correction calculated with trajectory modeling), and 5% from relative form factor uncertainty. The total expanded uncertainty at a comparable confidence level is the quadrature sum of the relative uncertainty and systematic contributions as follows: uncertainty in the metastable fraction of the ion beam (20% for C^{2+}, 15% for N^{3+}, 14% for O^{4+}), spatially delimiting the signal on the detector (3%), subtraction of the below threshold signal (6% for C^{2+}, 9% for N^{3+}, 11% for O^{4+}), detector efficiency (4%), absolute form factor (12%), and ion and electron current measurements (1% each). Uncertainties in the ion and electron velocities and dead times of the detector and electronics are negligible compared to the above uncertainties given in parentheses.

3 Theory

The theoretical CCR results are obtained in a six-state R-matrix calculation [14], that is all $2s^2$, 2s2p and $2p^2$ states are explicitly included. These states are represented by configuration interaction wavefunctions formed from bound 1s, 2s, and 2p orbitals augmented with 3s, 3p, 3d, and 4f pseudo orbitals, as described previously [14]. (A full description of the atomic R-matrix computations is given in Berrington *et al.* [24].) Twelve continuum terms per scattering channel are used in the scattering calculation in the inner region expansion; in the outer region, perturbed Coulomb functions are employed to account for the long-range dipole potentials. The partial-wave expansion is truncated at $L = 10$, and augmented with a “top-up” even though all of the transitions are reasonably well converged by $L = 10$ at the (low) energies of interest here. Top-up involves the extrapolation to infinity of the partial cross section from the highest L explicitly included, assuming a geometric series for allowed transitions; no extrapolation is done, nor is necessary, for other transitions. Because of the low energy range of the present calculations, the omission of $n = 3$ and higher states in the close-coupling expansion does not introduce significant errors in the cross sections reported here. This was verified by comparison with previous calculations [25,26] that included the $n = 3$ terms.

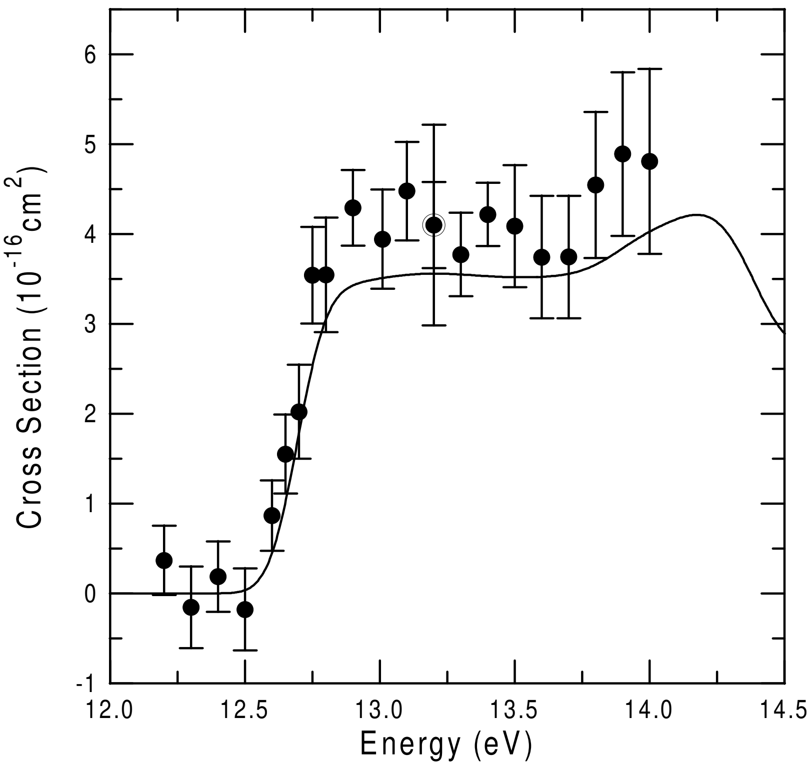

Fig. 3. Cross sections for electron-impact excitation of the $2s^2\ ^1S \to 2s2p\ ^1P^o$ transition in C^{2+} as a function of the center-of-mass energy. The points are the present data with 90% confidence level relative error bars. The outer error bars on the point at 13.2 eV represent the total expanded uncertainty. The solid curve is the present CCR calculation convoluted with a 0.23 eV FWHM Gaussian representing the experimental electron energy distribution. The calculations have been shifted to the spectroscopic threshold for comparison with the measurements. The experimental cross sections have been corrected for a metastable fraction of 0.56 (see text for explanation).

4 Results

4.1 $2s^2\ ^1S \to 2s2p\ ^1P^o$

The measured cross sections for this dipole transition from the ground state of C^{2+} are shown in Fig. 3 along with the results of the present CCR calculation. The experimental data (circles) are presented with relative error bars at the 90% confidence level, with the outer bars on the point at 13.2 eV representing a typical total expanded uncertainty (27%) of the measurements. The solid curve shown in Fig. 3 is the convolution of the present CCR calculations with a 0.23 eV FWHM Gaussian representing the experimental electron energy distribution. The agreement between the experimental and theoretical cross sections is very good in both magnitude and shape, well within the total

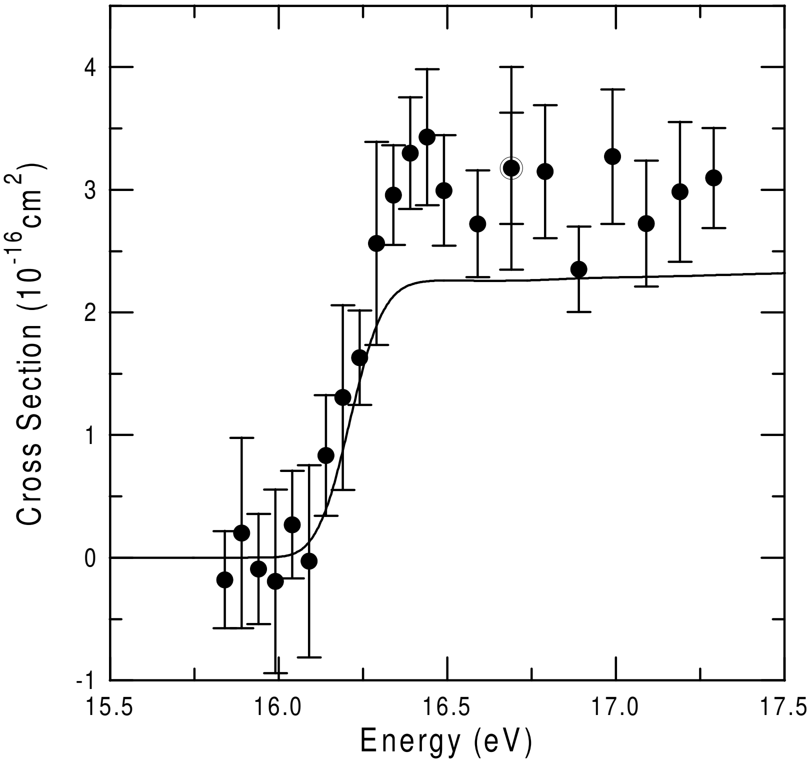

Fig. 4. Cross sections for electron-impact excitation of the $2s^2\ ^1S \rightarrow 2s2p\ ^1P^o$ transition in N^{3+} as a function of the center-of-mass energy. The points are the present data with 90% confidence level relative error bars. The outer error bars on the point at 16.7 eV represent the total expanded uncertainty. The solid curve is the present CCR calculation convoluted with a 0.18 eV FWHM Gaussian representing the experimental electron energy distribution. The calculations have been shifted to the spectroscopic threshold for comparison with the measurements. The experimental cross sections have been corrected for a metastable fraction of 0.52 (see text for explanation).

expanded uncertainty of the measurements. The MEIBEL results above 13.3 eV have been corrected for backscattering and other signal losses as discussed previously.

Experimental and theoretical cross sections for excitation of the first allowed transition from the ground state of N^{3+} are presented in Fig. 4. Again, the MEIBEL results are shown as circles, with 90% confidence level relative error bars. A typical total expanded uncertainty (26%) of the measurement is indicated by the outer error bars on the point at 16.7 eV. Measured cross sections for energies greater than 16.9 eV have been corrected for signal loss. The CCR results are convoluted with a 0.18 eV FWHM Gaussian to represent the experimental electron energy distribution and plotted as the solid curve in Fig. 4. The agreement between theory and experiment is fair, with the experimental results lying about 25% above the CCR predictions. This discrepancy may be due to having a metastable fraction of the N^{3+} ion beam that is less than the

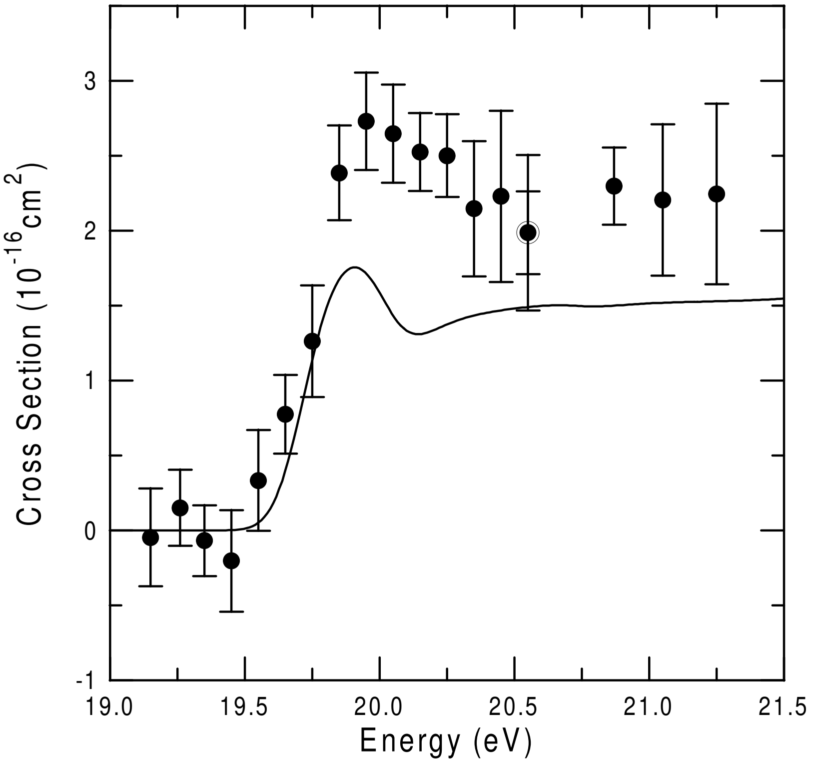

Fig. 5. Cross sections for electron-impact excitation of the $2s^2\ ^1S \rightarrow 2s2p\ ^1P^o$ transition in O^{4+} as a function of the center-of-mass energy. The points are the present data with 90% confidence level relative error bars. The outer error bars on the point at 20.55 eV represent the total expanded uncertainty. The solid curve is the present CCR calculation convoluted with a 0.22 eV FWHM Gaussian representing the experimental electron energy distribution. The calculations have been shifted to the spectroscopic threshold for comparison with the measurements. The experimental cross sections have been corrected for a metastable fraction of 0.42 (see text for explanation).

value of 0.52 measured by Brazuk *et al.* [17]. A metastable fraction of roughly 0.4 would yield the best agreement between the theoretical and experimental cross sections.

Figure 5 shows the cross sections, measured and calculated, for the $2s^2\ ^1S \rightarrow 2s2p\ ^1P^o$ transition in O^{4+}. The solid curve is the present close-coupling prediction convoluted with a 0.22 eV FWHM Gaussian representing the energy distribution of the electrons. The experimental data, shown as circles, are displayed with 90% confidence level relative error bars. The outer error bars on the point at 20.55 eV indicate a typical total expanded uncertainty (26%) for the measurements. Above 20.35 eV the experimental results include corrections for backscattering and other signal losses.

The experiment and theory for the first allowed transition in O^{4+} do not agree within the total expanded uncertainty for most of the measurements.

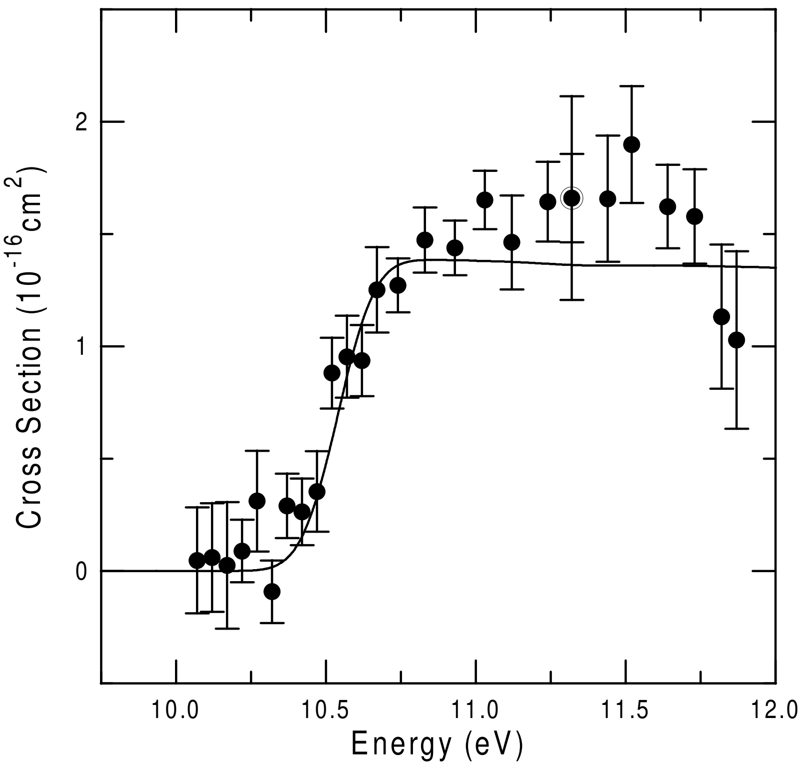

Fig. 6. Cross sections for electron-impact excitation of the 2s2p ^{3}P^o $\rightarrow$ 2p^2 ^{3}P transition in C^{2+} as a function of the center-of-mass energy. The points are the present data with 90% confidence level relative error bars. The outer error bars on the point at 11.3 eV represent the total expanded uncertainty. The solid curve is the present CCR calculation convoluted with a 0.23 eV FWHM Gaussian representing the experimental electron energy distribution. The calculations have been shifted to the spectroscopic threshold for comparison with the measurements. The experimental cross sections have been corrected for a metastable fraction of 0.56 (see text for explanation).

Instead, the MEIBEL measurements lie about 40% above the CCR predictions. As discussed previously for N^{3+}, one possible source of discrepancy is the metastable fraction of 0.42 adopted from Brazuk *et al.* [17]. If the metastable fraction were 0.30, the agreement between experiment and theory would be excellent. The experimental data are consistent with the resonance feature of the theoretical curve.

4.2 2s2p $^3P^o \rightarrow 2p^2$ ^3P

For C^{2+}, we also present results for the first parity-allowed transition from the metastable 2s2p ^{3}P^o level. The experimental cross sections, shown as circles in Fig. 6, are presented with 90% confidence level error bars. The outer error bar on the point at 11.3 eV indicates a typical total expanded uncertainty for the

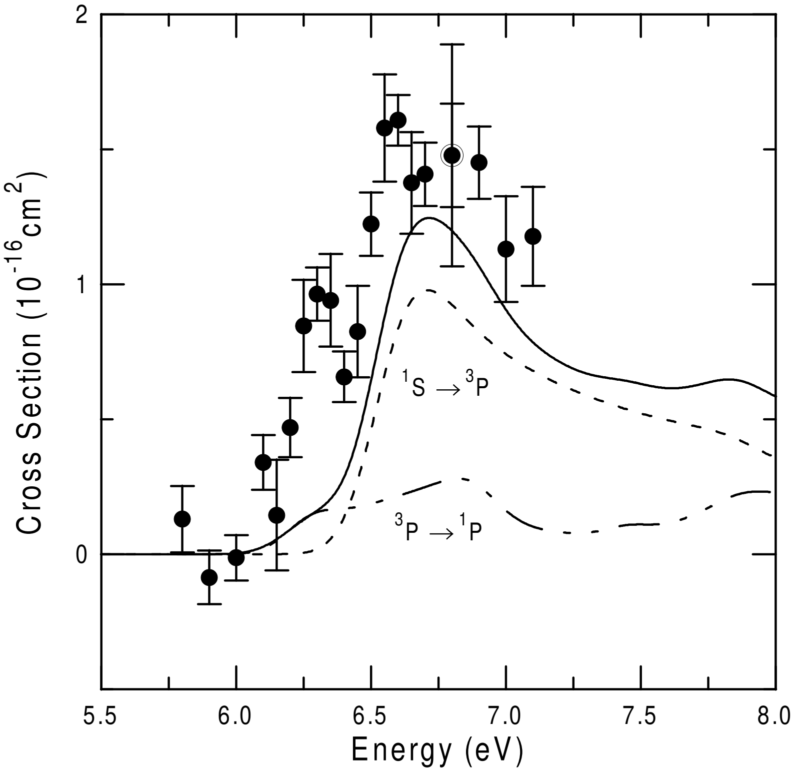

Fig. 7. Cross sections for electron-impact excitation of the 2s2p $^3P^o \rightarrow$ 2s2p $^1P^o$ and 2s^2 ^{1}S $\rightarrow$ 2s2p $^3P^o$ transitions in C^{2+} as a function of the center-of-mass energy. The points are the present data with 90% confidence level relative error bars. The outer error bars on the point at 6.8 eV represent the total expanded uncertainty. The curves are the present CCR calculations, each convoluted with a 0.23 eV FWHM Gaussian representing the experimental electron energy distribution, with the calculations for the $^3P^o \rightarrow {}^1P^o$ transition (dot-dash) scaled by 0.56 to account for the metastable fraction of the target ions. Similarly, the calculations for ^{1}S $\rightarrow$ $^3P^o$ transition (dashed) have been scaled by 0.44 to account for the ground state fraction. The sum of the two scaled CCR calculations is shown as the solid curve.

measurements. Corrections applied to the measured cross sections above 10.9 eV to account for signal loss (discussed in Section 2) are 3% or less except at the four highest energies measured. The close-coupling calculations are convoluted with a 0.23 eV FWHM Gaussian representing the electron energy distribution and plotted as the solid curve in Fig. 6. Good agreement is seen between the measured and calculated cross sections.

4.3 2s^2 $^1S \rightarrow$ 2s2p $^3P^o$ and 2s2p $^3P^o \rightarrow$ 2s2p $^1P^o$

The metastable 2s2p $^3P^o$ level in C^{2+} lies just over half-way between the 2s^2 ^{1}S ground state and the 2s2p $^1P^o$ level, so the thresholds for the 2s2p $^3P^o$ $\rightarrow$ 2s2p $^1P^o$ and 2s^2 ^{1}S $\rightarrow$ 2s2p $^3P^o$ transitions differ by only 0.31 eV (see Fig. 2). These two transitions cannot be resolved in the MEIBEL technique for the reason stated in Section 2. Shown in Fig. 7 are the experimental cross sections (circles) that have not been corrected for the metastable fraction of the ion beam since above the $^3P^o \rightarrow {}^1P^o$ threshold, both ground state and metastable ion targets contribute to the measured signal. Instead, the theoretical predictions for each transition are scaled for comparison with the measurements. The error bars shown represent the relative uncertainties at the 90% confidence level except the outer error bars on the point at 6.8 eV that indicate a typical total expanded uncertainty. Signal-loss corrections have been applied to the measurements above 6.7 eV. The dash-dot and dashed curves in Fig. 7 are the convolutions of the CCR calculations for the $^3P^o \rightarrow {}^1P^o$ and $^1S \rightarrow {}^3P^o$ transitions, respectively, with a Gaussian of 0.23 eV FWHM representing the electron energy distribution. The $^3P^o \rightarrow {}^1P^o$ predictions have been multiplied by the metastable fraction of 0.56 for comparison with the experiment. Similarly, the $^1S \rightarrow {}^3P^o$ calculations have been scaled down by the ground state fraction of 0.44. The solid curve is the sum of the two scaled CCR calculations.

Above the $^1S \rightarrow {}^3P^o$ threshold, the agreement between theory and experiment is fairly good for the combined cross sections. However, the measured cross sections show a resonance feature just above the threshold for the $^3P^o \rightarrow {}^1P^o$ spin-forbidden transition. Further study is required to decide whether the CCR approach predicts that the energy of the associated doubly-excited state of C^+ lies just below the excitation threshold so that it does not contribute. Similar discrepancies about positions of dielectronic resonances have been reported previously [9,10] and are not surprising considering how sensitive the CCR results are to the structure calculations of the doubly-excited intermediate states [27,28]. A more sophisticated calculation with much more correlation including core polarization may be necessary to obtain complete consistency between the target state and resonant state energies.

For O^{4+}, as with C^{2+}, the 2s2p $^3P^o \rightarrow$ 2s2p $^1P^o$ and 2s^2 $^1S \rightarrow$ 2s2p $^3P^o$ transitions cannot be resolved by the MEIBEL technique. Hence, the CCR results shown in Fig. 8 for the $^3P^o \rightarrow {}^1P^o$ transition (dot-dash curve) have been multiplied by 0.42 to account for the metastable fraction of the target ions and convoluted with a 0.22 eV FWHM Gaussian representing the experimental electron energy distribution. Similarly, the CCR calculations for the $^1S \rightarrow {}^3P^o$ transition (dashed curve) have been convoluted and scaled down by the ground state fraction of 0.58. The solid curve is the sum of the two scaled CCR predictions. The MEIBEL results are presented as circles, with 90% confidence level error bars and include signal-loss corrections above 10.65 eV. The outer bars on the point at 10.8 eV indicate a typical total expanded uncertainty of the measurements. As discussed above for these unresolved transitions in C^{2+}, the experimental results have not been corrected for the metastable fraction of the target O^{4+} ions.

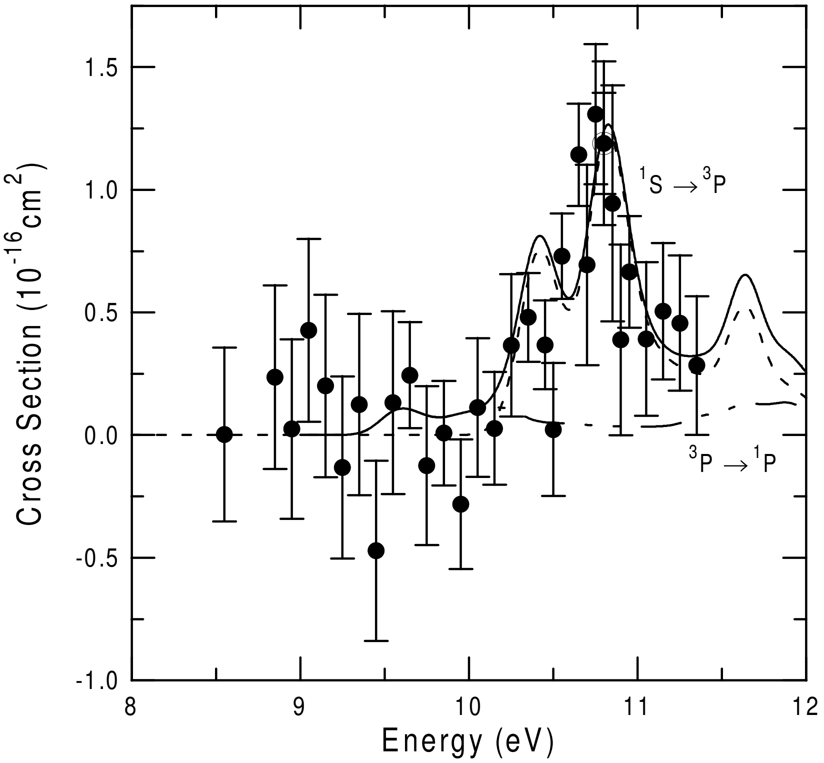

Fig. 8. Cross sections for electron-impact excitation of the 2s2p $^3P^o \to$ 2s2p $^1P^o$ and $2s^2$ $^1S \to$ 2s2p $^3P^o$ transitions in O^{4+} as a function of the center-of-mass energy. The points are the present data with 90% confidence level relative error bars. The outer error bars on the point at 10.8 eV represent the total expanded uncertainty. The curves are the present CCR calculations, each convoluted with a 0.22 eV FWHM Gaussian representing the experimental electron energy distribution, with the calculations for the $^3P^o \to {}^1P^o$ transition (dot-dash) scaled by 0.42 to account for the metastable fraction of the target ions. Similarly, the calculations for $^1S \to {}^3P^o$ transition (dashed) have been scaled by 0.58 to account for the ground state fraction. The sum of the two scaled CCR calculations are shown as the solid curve.

The agreement between the CCR calculations and the MEIBEL measurements are reasonable over the entire energy range. However, the predicted cross sections for the $^3P^o \to {}^1P^o$ transition are smaller than the relative uncertainties of the measurements so little is learned about this particular excitation. The resonance feature measured near 10.8 eV is accurately predicted by the CCR theory for the $^1S \to {}^3P^o$ transition.

5 Conclusions

The merged electron-ion beams energy-loss technique has been used to measure electron-impact excitation cross sections for both dipole-allowed and forbidden transitions from the ground and metastable states of Be-like C^{2+}, N^{3+}, and O^{4+} ions. The present close-coupling R-matrix (CCR) calculations are benchmarked against these measurements. Using the metastable ion fractions measured by Brazuk *et al.* [17], satisfactory agreement between theory and experiment is seen for the allowed transitions, although the measurements for the $2s^2\ ^1S \rightarrow 2s2p\ ^1P^o$ transition in N^{3+} and O^{4+} lie about 30% and 40% higher than the theoretical predictions, respectively. In order to eliminate the possibility of cross section discrepancies due to metastable ion fractions in the present experiment differing from those reported by Brazuk *et al.*, another method of determining the metastable fraction must be implemented since the ionization cross section approach used previously [10,11] has proved unreliable for these Be-like ions. For the forbidden transitions, the agreement between the MEIBEL and CCR results is reasonable except for a measured resonance in the $^3P^o \rightarrow {}^1P^o$ transition in C^{2+} not predicted by theory. More benchmark measurements are needed, particularly for forbidden transitions, for a variety of ions common in laboratory and astrophysical plasmas, to continue the refinement of the close-coupling R-matrix approach that is relied upon for production of the bulk of required electron-impact excitation cross sections.

Acknowledgements

This research was supported by the Office of Fusion Energy Sciences of the U.S. Department of Energy under Contract No. DE-AC05-96OR22464 with Lockheed Martin Energy Research Corp. and Contract No. DE-A102-95ER54293 with the National Institute of Standards and Technology.

References

[1] W. P. West *et al.*, Plasma Phys. Control. Fusion **39** (1997) A295.

[2] R. E. S. Clegg, P. J. Storey, J. R. Walsh, and L. Neale, Mon. Not. R. Astron. Soc. **284** (1997) 348.

[3] W. A. Feibelman, Astrophys. J. **506** (1998) 773.

[4] M. G. Allen, M. A. Dopita, and Z. I. Tsvetanov, Astrophys. J. **493** (1998) 571.

[5] R. M. González Delgado, T. Heckman, C. Leitherer, G. Meurer, J. Krolik, A. S. Wilson, A. Kinney, and A. Koratkar, Astrophys. J. **505** (1998) 174.

[6] K. A. Berrington, At. Data Nucl. Data Tables **57** (1994) 71.

[7] C. A. Ramsbottom, K. A. Berrington, and K. L. Bell, At. Data Nucl. Data Tables **61** (1995) 105.

[8] D. C. Griffin, M. S. Pindzola, and N. R. Badnell, Phys. Rev. A **47** (1993) 2871.

[9] M. E. Bannister, X. Q. Guo, T. M. Kojima, and G. H. Dunn, Phys. Rev. Lett. **72** (1994) 3336.

[10] Y.-S. Chung, N. Djurić, B. Wallbank, G. H. Dunn, M. E. Bannister, and A. C. H. Smith, Phys. Rev. A **55** (1997) 2044.

[11] B. Wallbank, N. Djurić, O. Woitke, S. Zhou, G. H. Dunn, A. C. H. Smith, and M. E. Bannister, Phys. Rev. A **56** (1997) 3714.

[12] E. K. Wåhlin, J. S. Thompson, G. H. Dunn, R. A. Phaneuf, D. C. Gregory, and A. C. H. Smith, Phys. Rev. Lett. **66** (1991) 157.

[13] S. J. Smith, K.-F. Man, R. J. Mawhorter, I. D. Williams, and A. Chutjian, Phys. Rev. Lett. **67** (1991) 30.

[14] K. A. Berrington, P. G. Burke, P. L. Dufton, and A. E. Kingston, J. Phys. B **10** (1977) 1465.

[15] E. W. Bell, X. Q. Guo, J. L. Forand, K. Rinn, D. R. Swenson, J. S. Thompson, G. H. Dunn, M. E. Bannister, D. C. Gregory, R. A. Phaneuf, A. C. H. Smith, A. Müller, C. A. Timmer, E. K. Wåhlin, B. D. DePaola, and D. S. Belić, Phys. Rev. A **49** (1994) 4585.

[16] J. L. Forand, C. A. Timmer, E. K. Wåhlin, B. D. DePaola, G. H. Dunn, D. Swenson, and K. Rinn, Rev. Sci. Instrum. **61** (1990) 3372.

[17] A. Brazuk, D. Dijkkamp, A. G. Drentje, F. J. de Heer, and H. Winter, J. Phys. B **17** (1984) 2489.

[18] J. Doerfert, E. Träbert, A. Wolf, D. Schwalm, and O. Uwira, Phys. Rev. Lett. **78** (1997) 4355.

[19] Yu. V. Ralchenko and L. A. Vainshtein, Phys. Rev. A **52** (1995) 2449.

[20] M. E. Bannister, Phys. Rev. A **54** (1996) 1435.

[21] S. M. Younger, Phys. Rev. A **24** (1981) 1278.

[22] SIMION 3D Version 6.0, David A. Dahl, Idaho National Engineering Laboratory.

[23] S. Bashkin and J. O. Stoner, Jr., Atomic Energy Levels and Grotian Diagrams, Vol. 1, North-Holland, Amsterdam, 1975, pp. 80-86.

[24] K. A. Berrington, W. B. Eissner and P. H. Norrington, Comput. Phys. Commun. **92** (1995) 290.

[25] C. A. Ramsbottom, K. A. Berrington, A. Hibbert and K. L. Bell, Physica Scripta **50** (1994) 246.

[26] K. A. Berrington, P. G. Burke, P. L. Dufton, A. E. Kingston, A. Sinfailam, J. Phys. B **12** (1979) L275.

[27] T. W. Gorczyca, M. S. Pindzola, N. R. Badnell, and D. C. Griffin, Phys. Rev. A **51** (1995) 488.

[28] N. R. Badnell, D. C. Griffin, T. W. Gorczyca, and M. S. Pindzola, Phys. Rev. A **50** (1994) 1231.